Lightweight ironless-stator PM generators for direct-drive wind turbines

E. Spooner, P. Gordon, J.R. Bumby and C.D. French

Abstract: A permanent-magnet electrical machine that employs lightweight spoked structures for both rotor and stator is described. The stator is ironless so that there is no direct magnetic attraction between rotor and stator. The lightweight structures are sufficient to carry the small forces due to the interaction of the permanent magnet field with the stator winding current. Despite the absence of stator iron and a large airgap, rare-earth magnets are able to create a working flux density of about 0.25 T at the winding. This is sufficient for an effective generator design because the lightweight structures offer the opportunity to build generators of unprecedented diameter. The outcome is a generator that has a mass typically 20–30% of equivalent designs based on iron-cored magnetic circuits, and with efficiency greater than 90%.

A	magnetic vector potential, Wb/m
B	flux density, T
C_P	power coefficient
J	current density, A/m^2
K	electric loading, A/m
L	inductance, H
P	power, W
P_{loss}	power loss per unit area, W/m^2
P_{eddy}	eddy current loss in conductors, W/m^3
R	turbine radius, m
T	torque, N m
ΔT	winding temperature rise, K
V	wind speed, m/s
Y	radial separation from rotor iron, m
d	wire diameter, m
g	airgap: magnet to coil copper, m
h	heat transfer coefficient, W m^{-2} K^{-1}
k	ratio: wind speed/rated wind speed
k_{fill}	coil copper fill factor
ℓ	active length, m
n	number of coils or phases
p	pole pairs
r	generator radius, m
t	winding radial thickness, m
u	pole pitch/π, m
β	turbine tip speed ratio
δ	torque angle, rad
λ	flux linkage, Wb
ρ	air density, kg/m^3
σ	shear stress, N/m^2
τ	normal stress, N/m^2
$\grave{u}$	angular speed, electrical angular frequency, rad/s

Mean values are indicated with a bar and peak values with a cap, e.g. $\bar{\sigma}, \hat{B}$

IEE Proceedings online no. 20041084

doi:10.1049/ip-epa:20041084

Paper first received 18th March and in revised form 5th August 2004

E. Spooner and J.R. Bumby are with the School of Engineering, University of Durham, UK

P. Gordon is with the Evolving Generation Ltd, School of Engineering, University of Durham, UK

C.D. French is with the Electrical Drives and Machines Group, University of Newcastle upon Tyne, UK

1 Introduction

Wind turbines rated up to about 5 MW, 12 rpm are being designed for offshore wind farms. The high unit cost of installation, foundations and offshore electrical network infrastructure motivate the urgent development of yet larger machines. Blades have until recently limited the development of larger machines because of stresses at the blade root and the visual impact of very large turbines. The prospect of carbon-fibre blades and the move toward offshore installation removes these barriers and blades of indefinite length appear feasible in principle [1]. Features such as drive trains, towers and foundations impose new barriers to increased ratings. The high cost of access for maintenance offshore creates a desire for direct-drive generators but the inevitably high weight of such machines would present severe difficulties for installation. A number of studies have taken place to develop concepts for large direct-drive wind turbine generators [2–5] and some examples have entered service with ratings up to 1.8 MW and a prototype machine of 4.5 MW has been installed [6–8]. These are all synchronous machines with wound-field or permanent-magnet excitation.

In all wind turbines rated at 1 MW or more, variable-speed operation is necessary so that the turbine inertia can absorb the energy of wind gusts without transmitting large transient loads into the supporting structure. The usual solution where the generator is driven via a gearbox at high speed (up to 1800 rpm) is to use a doubly-fed generator in which the rotor is supplied with variable frequency AC via sliprings from a bi-directional AC–DC–AC converter rated at about 30% of the turbine power. Direct-drive generators,

having permanent-magnet or wound-field excitation require fully-rated converters.

The new direct-drive generator concept is a permanent-magnet machine that overcomes the weight problem; it also has features that offer potential for the development of low-cost modular converters, giving a high degree of fault tolerance.

2 Proposed configuration

The proposed arrangement, illustrated in Figs. 1 and 2, uses a pair of spoked wheels to carry the rotor and stator of a radial-flux permanent-magnet machine. The rotor is a steel rim with rare-earth permanent magnets for excitation. The stator coils are fixed to non-metallic supports. The stator structure may be a lightweight composite structure in, say, glass fibre. Alternatively, an underlying structure in steel is acceptable provided that none of its parts is sufficiently close to the passing rotor magnets to be influenced either by magnetic forces or eddy currents; a clearance of about two pole pitches should be satisfactory. The absence of iron in the stator avoids the radial attractive force so that the lightweight spoked structures are stiff enough to provide the necessary support. Several variations on this basic form are possible in which the rotor is placed inside or outside the stator. The discussion centres on the arrangement shown in Fig. 3, in which the rotor and stator wheels are nested with the rotor wheel enclosing the stator wheel. The auxiliary thrust bearing is required to react the axial component of the force in the rotor spokes; it does not need to be centred and a simple ring running on light rollers or castors may be adequate.

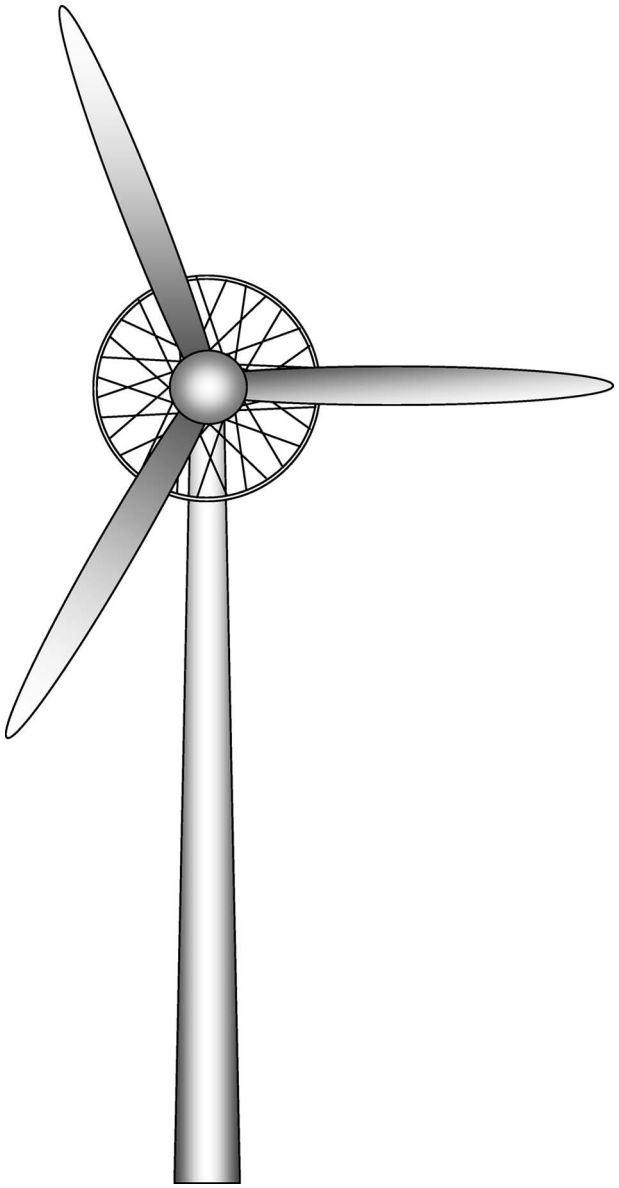

Fig. 1 *Wind turbine with proposed generator*

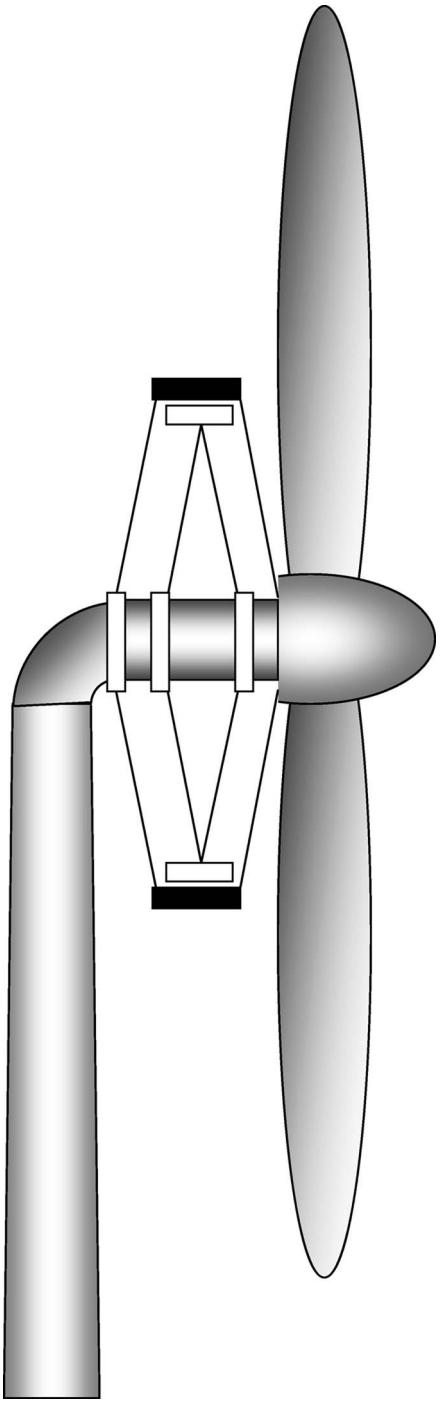

Fig. 2 *Arrangement of generator on turbine*

Figure 4 shows a possible cross-section of the two rims. If the stator coils are arranged to be detachable as illustrated then they may be replaced if necessary. The coils feed a DC busbar via individual diode rectifiers.

The stator and rotor spoke and rim structures are both made of steel to avoid differential expansions. Ambient temperature changes would otherwise lead to possible

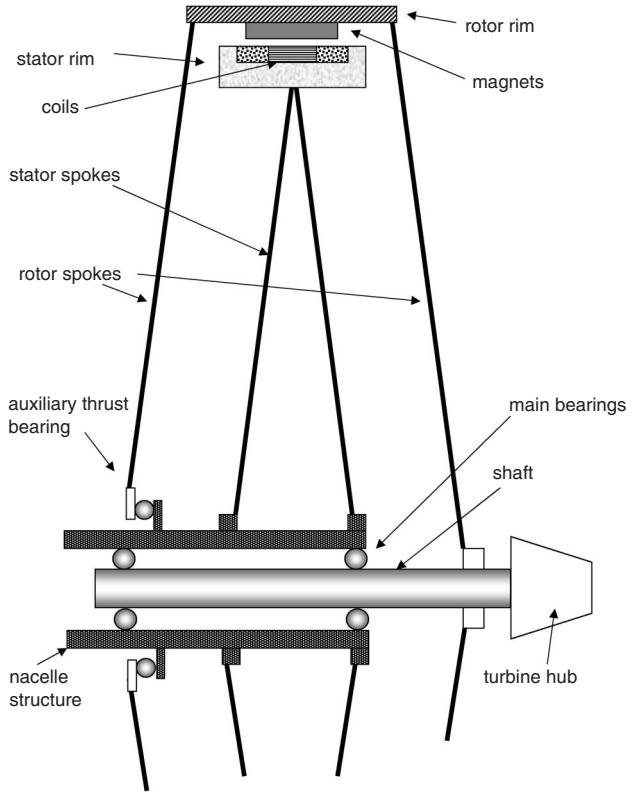

Fig. 3 *Overall generator cross-section*

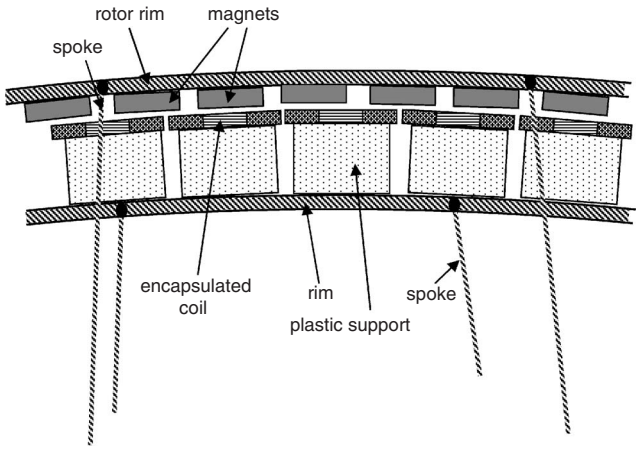

Fig. 4 *Cross-section of rotor and stator rim*

closure of the airgap and damage to coils. The stresses in the spokes and rims are carefully adjusted at the design stage to enable the torque to be developed without causing any spokes to become slack. Differential expansion between spoke and rim would have an adverse effect on this condition and call for increased pre-stressing of the structure and consequently greater mass.

Designs based on the use of circular magnets and coils have been considered earlier [9], these are simple to build and the calculation of their parameters is relatively simple. However, to create designs having acceptable diameter, it is necessary for the active length to be rather greater than the pole pitch, thus designs based on rectangular magnets are preferred. The rotor magnets are rectangular blocks, and in most designs, much larger than can be obtained as a single piece. Magnetising and handling these components is a significant practical challenge. In situ magnetisation after assembly of most of the generator components is desirable and some progress has been made with regard to large iron-cored machines [10] although for much smaller magnets than are needed for the ironless machine.

The stator winding uses coils of simple racetrack form. The number of coils is chosen to allow the stator to be divided into arcs for transport and to differ from the pole number so that the outputs are not co-phasal. For protection from the elements, the coils are encapsulated either individually and fixed to the supporting structure or they may be embedded within the structure itself. The coils are mounted side by side and each produces a single-phase AC output. The coils are well isolated by their encapsulation and since their outputs are combined only after rectification by diodes, a high degree of fault tolerance is possible. In the alternative arrangement where overlapping coils form a polyphase winding it is difficult to divide the machine into segments for transport and the coils are thermally and electrically close coupled so that a single coil fault could disable the entire machine. The high cost of access to an offshore turbine places a high value on reliability and fault tolerance. Indeed, a convincing case could be made for building the machine with some excess capacity and leaving faults unrepaired.

3 General principles

3.1 Torque production

A wind turbine operating in a wind of speed V produces power equal to:

$$P = \frac{1}{2}\rho V^3 \pi R^2 C_P \tag{1}$$

at a rotational speed of

$$\omega = \frac{V\beta}{R} \tag{2}$$

At the optimum value of β, the tip speed ratio, the power coefficient, C_P, reaches its maximum value of typically 0.47. The torque, obtained by dividing (1) by (2), is proportional to the cube of the turbine radius:

$$T = \frac{\pi\rho V^2 R^3 C_P}{\beta} \tag{3}$$

The generator must produce an equal torque. A radial-flux electrical machine produces torque:

$$T = \bar{\sigma}.2\pi r^2 \ell \tag{4}$$

If the distributions of flux density and electric loading are sinusoidal with a relative displacement δ and peak values $\hat{B}$ and $\hat{K}$, respectively, then the mean shear stress at the airgap, $\bar{\sigma}$, is

$$\bar{\sigma} = \frac{1}{2}\hat{B}\hat{K}\cos\delta \tag{5}$$

The proposed machine produces torque according to (4) by way of a low value of shear stress compensated for by an unusually large radius. The low shear stress results from the absence of stator iron leading to a low airgap flux density.

3.2 Generator dimensions

Equating turbine and generator torque yields the ratio of generator radius to turbine radius:

$$\frac{r}{R} = V\sqrt{\frac{\rho C_P}{\beta\hat{B}\hat{K}\cos\delta(\ell/r)}} \tag{6}$$

Taking typical values for large wind turbines as given in Table 1 gives a ratio of 0.285. So, for example, a 100 m diameter turbine would require a generator of 28.5 m

Table 1: Typical wind turbine and generator parameters

Air density	ρ	kg/m^3	1.22
Rated wind speed	V	m/s	13
Power coefficient	C_P		0.47
Tip speed ratio	β		5.5
Ratio generator active length to radius	ℓ/r		0.02
Effective airgap flux density	$\hat{B}$	T (peak)	0.25
Electric loading	$\hat{K}$	kA/m (peak)	50

diameter, with 570 mm active length, which would be manageable for the same plant used to erect the turbine itself. The tabulated data correspond to a rating of 4.9 MW at 13.7 rpm.

3.3 Mass of active material

The active material includes the magnets, the winding and the back iron. In most conventional machines the stator and rotor back iron are the largest components of the mass. The thickness of back iron required for magnetic purposes is determined by the pole pitch and the working flux density. For the proposed machine, the stator has no back iron and little back iron is required for the rotor because of the low flux density.

Figure 5*a* and *b* compare the active masses of the ironless generator with slotted- and slotless-stator radial-flux machines in terms of shear stress and efficiency. In each case a range of designs has been generated for the purpose of display, the data employed being as listed in Table 2. The generator/turbine diameter ratio for the slotted and slotless stator machines is taken to be 8%,which is typical of commercial examples. The efficiency reaches values of up to about 95%, which is rather lower than might be expected for machines of 5 MW power capacity, and is a direct consequence of the low rotational speed.

It is observed from the distributions of these populations that:

- The ironless machine offers a similar ratio of shear stress to active mass as a conventional slotted machine.
- The slotless machine offers the best ratio of shear stress to active mass.
- The ironless machine offers a higher ratio of power to active mass than the other types. This is arises because of its larger diameter.
- The ironless machine can be as efficient as a slotted machine and better than a slotless machine.

3.4 Mass of structural materials

In some designs the back iron serves as the main structural member resisting deformation due to the magnetic force across the gap, and its thickness may need to be increased for this purpose beyond the straightforward magnetic requirement. The structure of an electrical machine serves two main functions: transmission of torque from the airgap region to the shaft and resisting the distorting forces that tend to close the airgap. Usually the latter function is much more demanding, and the structural design is dominated by the need to resist the direct attraction between the rotor and stator magnetic iron parts. In the ironless machine, however, there is no direct magnetic attraction between rotor and stator and so a very lightweight structure is sufficient.

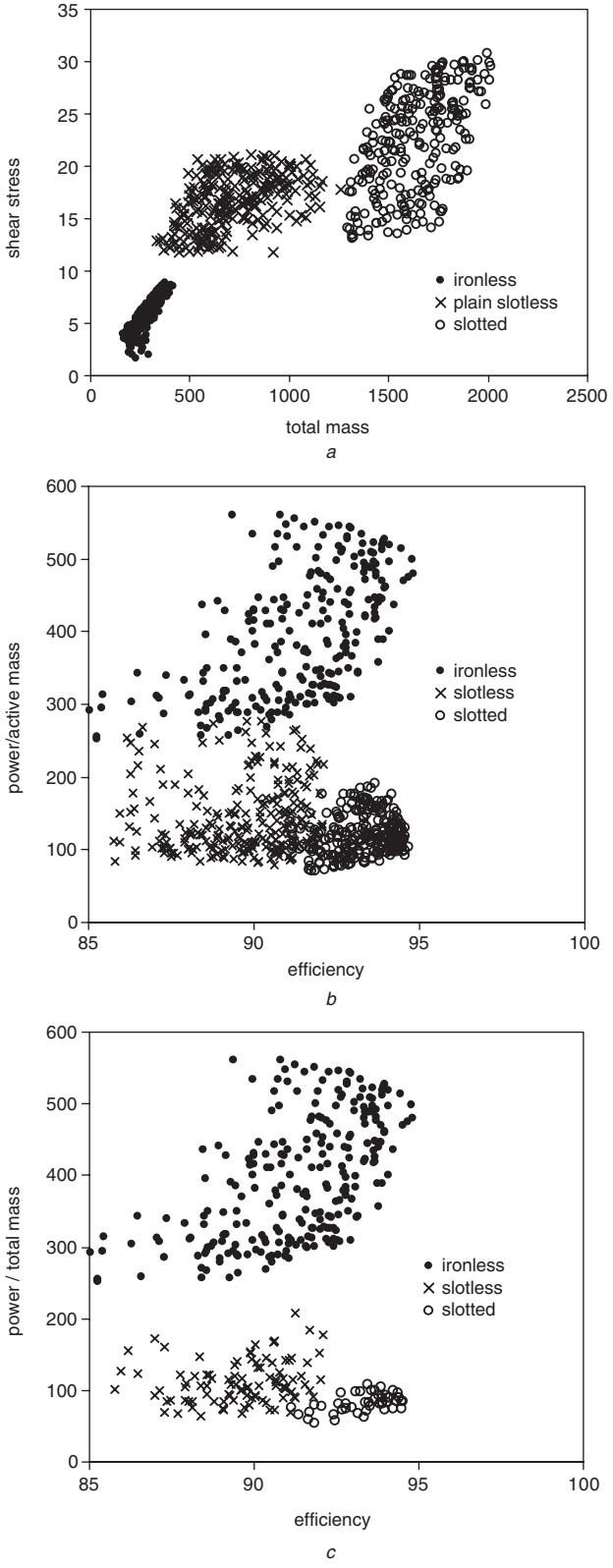

Fig. 5 *Comparison of power, mass and efficiency for alternative machines*

A lower limit to the necessary structural mass required by other types is that which is necessary for the structure to provide sufficient stiffness in the ovalising mode to overcome the negative stiffness associated with the permanent-magnet field. This is very sensitive to the machine diameter and to the radial depth of the supporting structure.

Figure 5*c* indicates the effect of this additional mass on the power to mass ratio for the case of a 100 m diameter turbine. The ironless machine clearly offers a distinct

Table 2: Data for comparative study

			Ironless	Slotless	Slotted
Generator / turbine dia	*r/R*		25%	8%	8%
Airgap	*g*	mm	15	6	6
Pole pitch	τ	mm	50–300	50–300	100–300
Magnet thickness		mm	10–25	10–25	10–25
Winding depth	*t*	mm	10–25	10–25	20–50
Wedge depth /slot width			–	–	0.5
Slot liner		mm	–	–	1
Loss per square metre	P_{loss}	kW/m^2	10	10	10
Magnet B rem		T	1.2	1.2	1.2
B back iron		T	–	1.4	1.4
B tooth		T	–	–	1.6

advantage for this size and the benefit increases with diameter.

4 Specific loadings

4.1 Magnetic loading

Figure 6, in which curvature has been exaggerated, illustrates the flux pattern created by a set of magnets fixed to the steel rim. The radial flux density distribution at the position of the winding is close to sinusoidal. Its amplitude is related to the magnet material, its thickness, the pole pitch and the distance between the magnets and the winding. The amplitude also varies with axial position because of the strong axial leakage fields at the ends of the magnets, as indicated in Fig. 7. In an idealised 2D model, the flux density decays exponentially with distance from the rotor steel. The decay constant is equal to $(1/\pi) \times$ the pole pitch. In the real situation the flux density decay is more rapid because of axial leakage at the ends. The flux density varies significantly through the thickness of the winding.

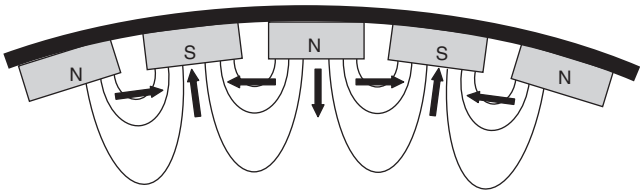

Fig. 6 *General flux pattern*

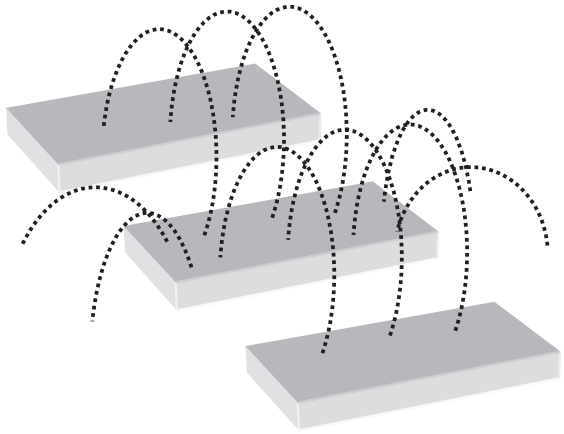

Fig. 7 *Magnet flux paths including end leakage*

For a particular example with a pole pitch of 200 mm, magnets 150 mm wide and 25 mm thick, made of sintered Nd–Fe–B having an energy product of 300kJ/m^3 (38MGOe), the flux density has a peak value of 0.26 T at a distance of 10 mm from the magnets decaying to 0.21 T at 30 mm. Doubling the magnet thickness increases these values by less than 50% to 0.36 and 0.30 T. It would be impractical to produce a flux density approaching the levels found in conventional iron-cored machines.

4.2 Electric loading

The electric loading may be restricted by either the temperature rise of the windings or by the reactance. Because of the flux density variation with distance from the magnets, the winding should not be made too thick otherwise the parts furthest from the magnets will contribute little to the useful torque but will make a full contribution to the I^2R loss and to the reactance.

If the electric loading is limited by the temperature rise, then, for a machine with simple air cooling at the stator surface, the winding loss per unit area of active surface P_{loss}, is determined. It is related to the temperature rise and a heat-transfer coefficient, *h*, that includes the effect of winding insulation and surface heat transfer to the surrounding air:

$$P_{loss} = h \times \Delta T \tag{7}$$

If the winding loss is entirely I^2R, then

$$P_{loss} = \frac{1}{2}\hat{J}^2 \rho \times t \times k_{fill} \tag{8}$$

So the electric loading is

$$\hat{K} = \hat{J} \times t \times k_{fill} = \sqrt{\frac{2h\Delta T k_{fill} t}{\rho}} \tag{9}$$

Now, the radial flux density varies from a maximum at the position closest to the magnets

$$\hat{B}_{\max} = \hat{B}_0 \exp\left(\frac{-g}{u}\right) \tag{10}$$

to a minimum at the furthest point

$$\hat{B}_{\min} = \hat{B}_0 \exp\left\{\frac{-(g+t)}{u}\right\} \tag{11}$$

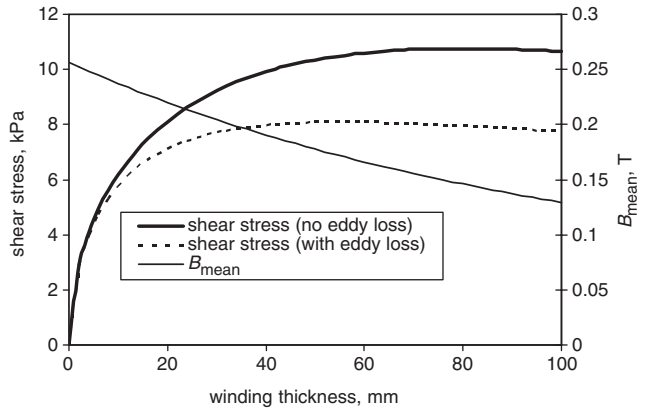

Fig. 8 *Effect of winding thickness on shear stress*
Winding fill factor 50%
Conductors 3 mm diameter
Temperature rise 100°C
Ambient 20°C
Heat transfer coefficient 60 W/m^{2}K
Pole pitch 200 mm
Clearance to magnets 10 mm
Flux density at magnet surface 0.3 T
Rotor surface speed 15 m/s

with a mean value

$$\hat{B}_{mean} = u\hat{B}_0 \exp\left(\frac{-g}{u}\right) \frac{\{1 - \exp(-t/u)\}}{t} \qquad (12)$$

The shear stress is the product of this value and the electric loading and it depends on the winding thickness, t, as illustrated in Fig. 8. In practice the winding loss includes a significant eddy current component as well as the I^2R loss. Increasing the winding thickness increases the amount of copper, and hence the eddy loss, so that the I^2R loss must be reduced to avoid an increase in temperature rise. The eddy current loss is determined by several factors such as the size and shape of the winding conductors. For round wires, diameter d, subjected to an alternating flux density normal to the wire, the eddy current loss per unit volume of conductor is:

$$P_{eddy} = \frac{\hat{B}^2\omega^2 d^2}{32\rho} \qquad (13)$$

An example is also plotted in Fig. 8 to illustrate the effect of the eddy current loss. Although the shear stress is maximum for a magnet thickness of 50 mm, it is apparent that there is little return in shear for increasing the winding thickness beyond about 20 mm in this case. The additional cost and weight of the extra 30 mm magnet thickness would negate the slight benefit due to the slightly higher shear stress.

5 Electrical parameters

5.1 EMF

The EMF is the rate of change of flux linkage as the rotor turns. The variation of flux density around the rotor has a fundamental component and harmonics. The harmonics decay with radius much more rapidly than the fundamental and are small at the position of the stator winding, the variation is therefore a reasonable sinewave. However, the third harmonic is noticeable and its effect can be beneficial. For the purpose of design, a procedure has been developed employing the polynomial modelling technique [11]. The technique produces the fundamental and low-order harmonics of the time variation of flux linkage in terms of the coil and magnet dimensions.

The EMF is affected by the number of turns in each coil and their distribution within the winding region. Turns at the inner part of the racetrack enclose less flux than those at the outer part and those furthest from the rotor enclose less than those closest. If the coil is significantly wider than the pole pitch then the outer turns will have lower flux linkage.

5.2 Reactance

The reactance is the result of the armature reaction flux. It is calculated from design dimensions using a 2D multilayer method as summarised in the Appendix, with a correction for the end turns based on the total area of an average turn compared with the area included in the straight section of the racetrack shape:

$$L_{eff} = L_{2D} \times \frac{A_{total}}{A_{straight}} \qquad (14)$$

Measurements of trial coils verify that this produces an accurate assessment of the reactance of the complete coil. Mutual inductance between adjacent coils causes the effective total inductance to be slightly greater than the inductance of a single isolated coil.

5.3 Rectifier load

It is assumed that the output from each coil feeds via a full-wave diode rectifier to a DC load that has constant voltage since a large number of similar coils with distributed phase feed the DC load in this way. The coils are electrically decoupled in a circuit of this type if the load has low effective input resistance. The coils, being mounted without overlap, have quite small mutual inductance and so it is reasonable to represent the entire system by a single typical coil and the DC load.

The current waveform, obtained by simulation, is illustrated in Fig. 9 for several cases having different ratios of DC to AC peak voltage and illustrating the beneficial effect of the third harmonic in extending the diode conduction period. The specifications for these simulated results are generally the same as for Fig. 8, the higher third harmonic being formed by extending the magnet width from 150 to 180 mm. The longer conduction period leads to a lower ratio of RMS coil current to DC current and to reduced winding loss.

6 Loss mechanisms

Losses in electrical machines are categorised as either load-dependent or constant. The main load loss is the I^2R loss in the winding. The principal constant loss in typical machines, the stator iron loss, is of course absent. However, two usually minor components assume much greater prominence. Eddy-current loss in the winding conductors is important because the conductors are subject to the main field, which has large tangential and axial components as well as the radial component that produces torque. Windage loss is potentially very serious because spokes have poor aerodynamic properties and there are a large number of them moving at high speed because of the large diameter of the machine. Indeed, the windage loss is one of the main considerations limiting the desirable radius of the generator.

The so-called constant losses are not truly constant, however. When the wind speed is less than the rated value, the turbine rotational speed is reduced to keep the tip speed

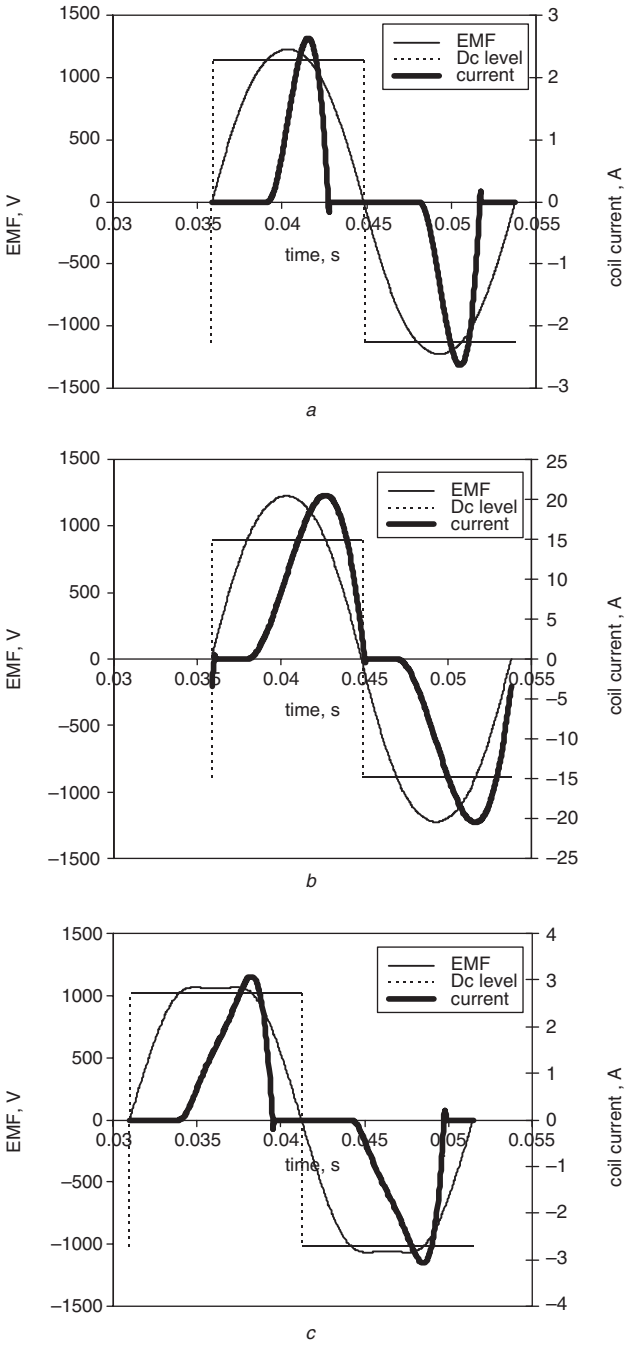

Fig. 9 *Coil current waveforms*
a $V_{dc} = 0.9\,V_{pk}$
b $V_{dc} = 0.7\,V_{pk}$
c $V_{dc} = 0.85\,V_{fund,pk}$ showing effect of third harmonic

ratio, β, at its ideal value. The frequency of the induced EMF that drives eddy currents is reduced and the eddy current loss is reduced according to the square of the wind speed. The aerodynamic drag on the rotor spokes and rim decreases as the square of speed and the power loss as the cube. Each loss component varies differently with wind speed; if the wind speed is $k \times$ the rated value ($k < 1$) then

- the shaft power varies as k^3
- the EMF varies as k
- the current varies approximately as k^2
- hence the I^2R loss varies approximately as k^4.
- the eddy current loss varies as frequency and hence as k^2
- the aerodynamic loss varies with the cube of speed, k^3.

It is interesting to note the losses that would occur in an equivalent iron-cored PM machine. Typically the iron loss is around half the I^2R loss at rated power and speed. Many electrical steels have specific iron loss that varies roughly as B^2 and $f^{1.3}$, i.e. as $k^{1.3}$, therefore at speeds less than 77% of rated the iron loss exceeds the I^2R. This is rather important because a wind turbine operates for long periods at speeds in this region. In compensation, the eddy current loss is greatly reduced by the screening effect of an iron core. Figure 10 compares the efficiency variation with speed for ironless and iron-cored machines having similar full-load efficiency.

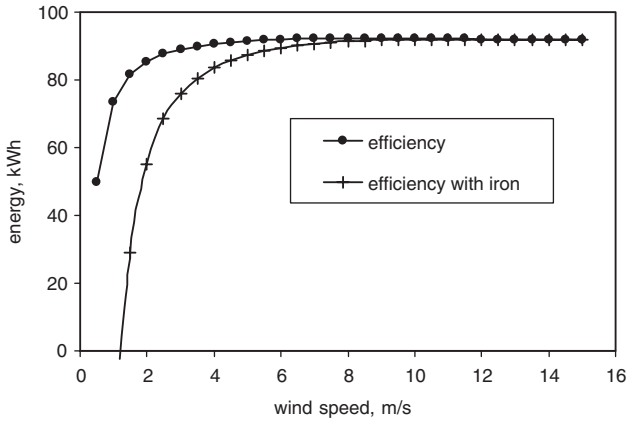

Fig. 10 *Efficiency comparison*
FL shaft power 5 MW
FL I^2R loss 200 kW
FL aerodynamic loss 100 kW
FL eddy loss 100 kW
FL iron loss 100 kW

Figure 11 shows the energy lost in a full year in a wind speed band of 0.5 m/s by the various mechanisms for typical values as listed. The wind speed is assumed to follow a Weibull probability density distribution with shape factor 2 and mean value 8 m/s which is typical for an offshore location.

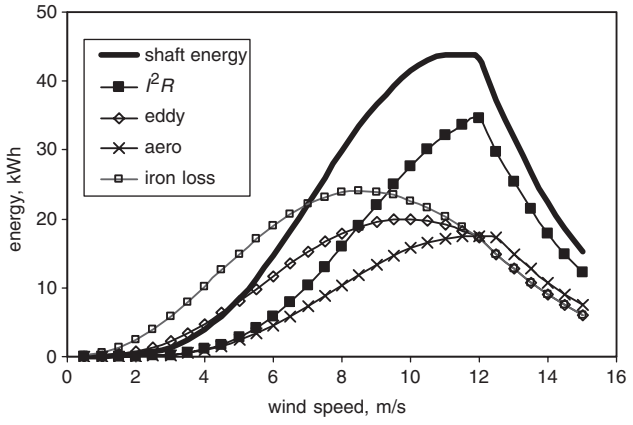

Fig. 11 *Energy generated and losses*
Shaft energy has been scaled by a factor 20 for illustration
Data as for Fig. 10

7 Fault conditions

7.1 Fault tolerance

The stator coils are well insulated from each other; this presents an opportunity to provide a good degree of fault

tolerance. The essential feature needed is to prevent a fault on one coil propagating electrically to others. The simplest way to accomplish this is to connect the coils via diodes, as proposed. It is perfectly natural to subdivide the set of coils to feed a number of DC loads so it would be possible to feed a number of relatively small isolated converters for grid interface. The converter outputs may be connected in parallel or in one of several possible multilevel configurations. With appropriate software, the system could be designed to tolerate the failure of one or more converter modules.

7.2 Forces during faults

The structure must withstand the forces present during fault conditions as well as normal operation. The airgap stress has a tangential component corresponding to the real power flow with mean value according to (5) and a maximum local value of

$$\sigma_{\max} = \bar{\sigma} + \frac{1}{2}\hat{B}\hat{K} \tag{15}$$

Owing to the absence of stator iron, the magnets produce a tangential flux density at the winding with amplitude equal to radial flux density and displaced by a half pole from the radial flux density distribution. There is, therefore, also a radial stress component with mean value

$$\bar{\tau} = \frac{1}{2}\hat{B}\hat{K}\sin\delta \tag{16}$$

and a maximum value of

$$\tau_{\max} = \bar{\tau} + \frac{1}{2}\hat{B}\hat{K} \tag{17}$$

It can be seen by comparing (5) and (16) that the shear stress corresponds to real power and the radial stress corresponds to reactive power developed in the stator winding. Under fault conditions in most machines, the current is limited mostly by the winding reactance and a substantial reactive power is consumed. The corresponding radial stress is therefore an important consideration for the structural design.

8 Laboratory prototype

8.1 Machine description

A demonstrator machine has been assembled and installed on the NaREC low-speed test facility at Durham University (Fig. 12*a*). The rotor magnets and stator coils are illustrated in Fig. 12*b*. The principal design data is given in Table 3. The stator is constructed from 12 arcs of 50 mm thick Tufnol held in compression by 48 spokes that are made of M6 threaded steel rod. The rotor is formed as a single ring from 150×6 mm mild steel and also uses 48 spokes of the same type.

The design has been prepared with the aid of a spreadsheet program that is used to prepare designs across the entire size range. A hypothetical turbine of 7.0 m diameter was adopted to create the specification. The predicted and measured electrical parameters are given in Table 4. Variations between coils lead to the variation in mean turn length and resistance.

8.2 Test results

The EMF induced in an individual coil was observed to be a good approximation to a sinewave as expected, Fig. 13*a*. The open circuit voltage obtained after rectification is plotted against speed in Fig. 13*b* along with the predicted characteristic. The slight excess in the measured voltage is

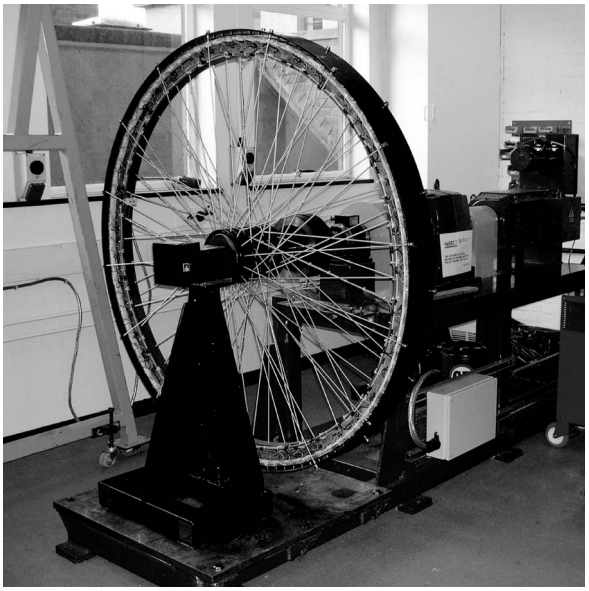

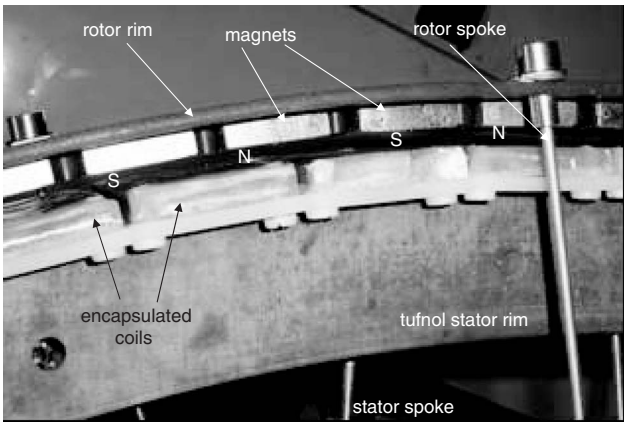

Fig. 12
a Prototype machine
b Prototype stator coil

Table 3: Prototype machine data

Nominal shaft power	KW	11.1
Nominal speed	RPM	150
Airgap diameter	m	1.74
Active (magnet) length	mm	80
Magnet thickness	mm	10
Pole number		108
Frequency at rated speed	Hz	135
Pole (magnet) width	mm	40
Pole pitch	mm	50
Airgap	mm	6
Stator coils		84
Coil outer width	mm	62
Coil inner width	mm	31
Coil resistance at 15°C	Ω	15.9
Coil effective reactance	Ω	25.8

believed to be caused by variations between coils causing some to lie closer to the rotor than intended, thereby having somewhat higher EMF. The electrical arrangement using diodes feeding a single common DC output causes the

Table 4: Predicted and measured electrical parameters

		Measured	Predicted
Coil EMF at 60 rpm	V RMS	99	105
Coil resistance at 15°C	Ω	16.5–16.9	15.9
Coil effective inductance	mH	26.5	24.4

output voltage to select the highest coil EMF. The same results, together with results from tests carried out under various load conditions and corresponding to predicted characteristics, are presented in Fig. 13*c*. Figure 13d shows a typical current waveform. The observed modulation is due to voltage ripple at the DC load. Under load conditions, the correspondence between predicted and measured voltage is better and it is believed that this is due to the load current flowing preferentially in the coils with highest EMF thus reducing their voltage to be closer to the average of all the coils. Similarly, less load current flows in those coils with lower EMF and they suffer less voltage drop. The predicted curves are based on the parameters calculated by the design spreadsheet. The correspondence between predicted and measured results validates the analysis that underlies the design procedures that have been developed.

Short circuit tests are difficult to carry out for permanent-magnet machines at their normal speed because the excitation cannot be reduced. Instead, a short-circuit test was carried out at very low speed to avoid excessive current and torque. For such a low speed the coil reactance is very low and the resistance is the dominant influence on the short-circuit current. The current is therefore very nearly in phase with the EMF and produces high torque. It is estimated that the torque produced was approximately 1100 Nm. The system of spokes and rim was designed for a nominal torque of 600 Nm and some distortion was observed during this test. The prevailing temperature of the coils is uncertain and Table 5 provides the measured current and a range of calculated currents corresponding to various winding temperatures. The calculation is clearly satisfactory for most purposes. Owing to its insensitivity to the coil inductance, the short-circuit test is not particularly informative for this machine and the earlier direct measurement of the inductance of an isolated coil is more useful and less stressful.

9 Conclusions

The proposed ironless-stator PM generator offers solutions to some of the serious problems facing the development of the offshore wind power industry. First, being a direct-drive machine, it overcomes the need for a gearbox with its associated maintenance demands. Secondly, the weight is very small in comparison with other forms of direct-drive generator and even with drive trains employing gearboxes. The weight reduction at the generator brings consequent economies in the tower and foundations. Lastly, it offers the prospect of creating a fault-tolerant electrical system through the use of modular inverters for interface to the grid.

Despite the absence of a stator iron core, the working flux density is sufficient for the machine to operate with very good electrical efficiency. One of the main loss components is the aerodynamic loss due to the large diameter.

A laboratory machine has been used to demonstrate the principal features and tests confirm the predicted performance characteristics.

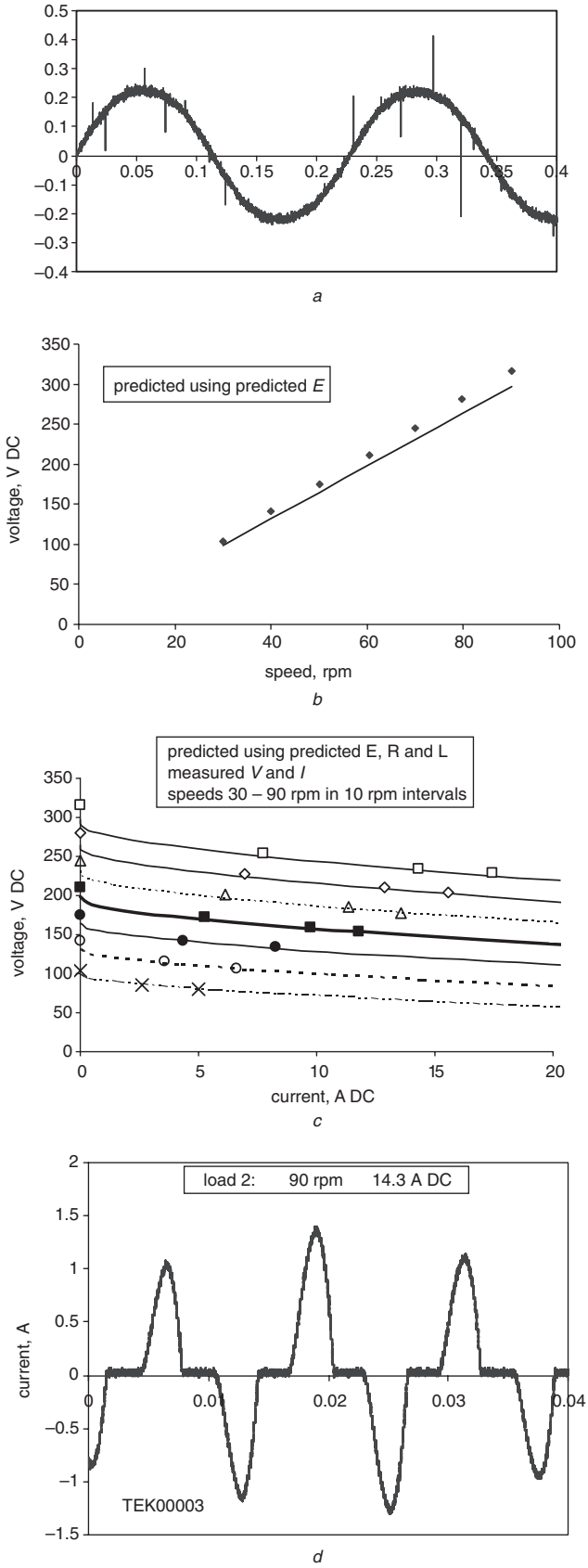

Fig. 13
a Coil EMF waveform
b No-load test results. Predicted line, measured points
c Load test results. Predicted curves, measured points
d Measured current waveform

10 Acknowledgments

The authors acknowledge the continuing support of the New and Renewable Energy Group in the School of

Table 5: Short-circuit test result and calculations

Test speed	rpm	16.8			
Measured S/C current	A	37.2			
Winding temperature	°C	30	40	50	60
Calculated S/C current	A	43.8	42.2	40.7	39.3

Engineering, University of Durham, and the active participation and financial support of the New and Renewable Energy Centre at Blyth Northumberland. The prototype machine was constructed by Fountain Design Ltd. of Bishop Auckland.

11 References

1 Millborrow, D.: 'No size constraint in size for wind turbines', *Wind Stats Newslett.*, Autumn 2002, **15**, (4)
2 Grauers, A.: 'Design of direct-driven permanent-magnet generators for wind turbines'. Technical report No. 292;, School of Electrical and Computer Engineering, Chalmers University of Technology, Goteborg, Sweden,1996
3 Spooner, E., Williamson, A.C., and Catto, G.: 'Direct-coupled permanent-magnet generators for wind-turbine applications', *IEE Proc. Eelectr. Power Appl.*, 1996, **143**, (1), pp. 1–8
4 Spooner, E., Williamson, A.C., and Catto, G. 'Modular design of permanent magnet generators for wind turbines', *IEE Proc. Eelectr. Power Appl.*, 1996, **143**, (5), pp. 388–395
5 Westlake, A.J.G., Bumby, J.R., and Spooner, E.: 'Damping the power angle oscillations of a permanent- magnet synchronous generator with particular reference to wind turbine applications', *lEE Proc. Electr. Power Appl.*, 1996, **143**, (3), pp. 269–280
6 http://enercon.de, accessed July 2004
7 http://www.jeumont-framatome.com, accessed July 2004
8 http://zephyros.com, accessed July 2004
9 Spooner, E.: 'Lightweight ironless PM generators for gearless wind turbines'. Presented at UK Magnetics Society Symp. 'New topologies for electrical machines', 2002, , De Montfort University, UK
10 Kang, D.H., Curiac, P., Jeong, Y.H., and Jung, S.J.: 'Prospects for magnetisation of large PM rotors: conclusions from a development case study', *IEEE Trans Energy Convers.*, 2003, **18**, (3), pp. 409–416
11 Hamlaoui, M.N., Mueller, M.A., Bumby, J.R., and Spooner, E.: 'Polynomial modelling of electromechanical devices – an efficient alternative to look-up tables', *IEE Proc. Electr. Power Appl.*, 2004, **151**, (6), pp. 758–768

12 Appendix

Inductance calculation by 2D multilayer method

The coils are assumed to be carrying a current of 1A(peak). with phase according to the EMF due to the magnets. The spatial distribution of current at some instant is decomposed into a fundamental and harmonics The inductance derived for each harmonic includes the effective contribution from mutual inductance. The configuration of Fig. 14 applies for each harmonic. The vector potential within

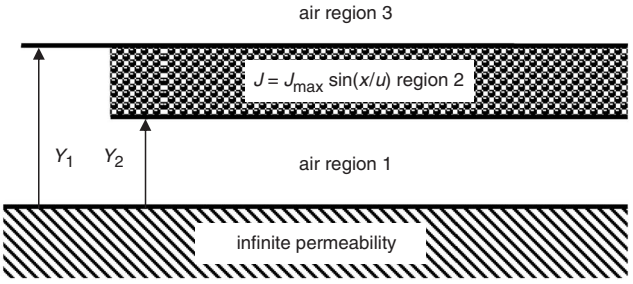

Fig. 14 *Multilayer model for inductance calculation*

region 2, the winding region is

$$A = \left\{A_{2,1}e^{\frac{y}{u}} + A_{2,2}e^{-\frac{y}{u}} + u^2\mu_0\hat{J}\right\}\sin\left(\frac{x}{u}\right) \tag{18}$$

In regions 1 and 3 similar expressions apply but with current density = 0. Boundary conditions are:

1 $H_x = 0$ at $y = 0$
2 continuity of A at Y_1
3 continuity of H_x at Y_1
4 continuity of A at Y_2
5 continuity of H_x at Y_2
6 $A = 0$ at infinite y.

From which values are derived $A_{1,1}$, $A_{1,2}$, $A_{2,1}$, $A_{2,2}$, $A_{3,1}$ and $A_{3,2}$, in particular:

$$A_{2,1} = -\frac{1}{2}u^2\mu_0\hat{J}e^{-\frac{Y_2}{u}} \tag{19}$$

$$A_{2,2} = -\frac{1}{2}u^2\mu_0\hat{J}\left(e^{\frac{Y_1}{u}} - e^{-\frac{Y_1}{u}} + e^{-\frac{Y_2}{u}}\right) \tag{20}$$

The product of current and flux linkage is given by

$$\lambda I = \iiint_{volume} AJdV \tag{21}$$

which is equal to

$$\lambda I = p\pi u\ell\hat{J}\left\{A_{2,1}u\left(e^{\frac{Y_2}{u}} - e^{\frac{Y_1}{u}}\right) + A_{2,2}(-u)\left(e^{-\frac{Y_2}{u}} - e^{-\frac{Y_1}{u}}\right)\right\} \tag{22}$$

Now for a balanced n-phase winding with inductance L per phase and no mutual inductances, carrying n-phase balanced current having peak value $\hat{I}$ the sum of the current flux linkage products for the n phases is

$$\lambda I = \frac{1}{2}nL\hat{I}^2 \tag{23}$$

which yields the effective inductance per phase. The total inductance is found by adding components for each space harmonic.